Possible Role of Lattice Dynamics in the Photocatalytic Activity of $BaM_{1/3}N_{2/3}O_3$ (M = Ni, Zn; N = Nb, Ta)

Jiang Yin,*,† Zhigang Zou,‡ and Jinhua Ye*,†,§

PRESTO, Japan Science and Technology Agency, 4-1-8 Honchou Kawaguchi, Saitama, Japan, Photoreaction Control Research Center (PCRC), Ecomaterials and Renewable Energy Research Center (ERERC), Nanjing University, 22 Hankou Road, Nanjing 210093, China, and Ecomaterials Center, National Institute for Materials Science (NIMS), 1-2-1 Sengen, Tsukuba, Ibaraki 305-0047, Japan

Received: October 21, 2003; In Final Form: April 26, 2004

New photocatalysts $BaNi_{1/3}M_{2/3}O_3$ (M = Nb, Ta) and $BaZn_{1/3}M_{2/3}O_3$ (M = Nb, Ta) with the ABO_3 perovskite structure were synthesized by the solid-state reaction method. They were characterized by X-ray diffraction, UV−vis reflectance spectroscopy, Raman spectroscopy, and photocatalytic activity measurement under UV light irradiation. Because of the same ionic radius of Nb^{5+} and Ta^{5+} in each pair, both compounds show the same lattice parameters. The Nb-containing photocatalyst with a narrower band gap and a smaller surface area shows a higher photocatalytic activity in evolving H_2 from the CH_3OH/H_2O solution under UV light irradiation than the Ta-containing photocatalyst. Some phonon modes in the bending branch of the Raman spectrum for the Ta-containing photocatalyst show an obvious red shift in their frequency, compared with those for the corresponding Nb-containing photocatalyst. It is suggested that these phonon modes play an important role in the migration of the charge carriers inside the photocatalysts, thus dominating their photocatalytic activities.

1. Introduction

In the past three decades, extensive efforts have been made to develop semiconductor photocatalysts that can split water into H_2 and O_2 under UV and visible light irradiation.[1−3] Of them, TiO_2 shows the most favorable conversion efficiency of solar energy. The most attention has been paid to understanding the reaction mechanism on the surface of the semiconductor and the charge migration between the semiconductor and the aqueous electrolyte.[4,5] As we know, the photocatalysis of the semiconductor includes the following basic processes: (1) electron−hole pairs are produced inside the semiconductor under photon irradiation with energy larger than that of the band gap; (2) some of the excited electrons and holes move to the surface of the semiconductor particles, and some of them recombine; and (3) a redox reaction of water molecules occurs on the surface of the semiconductor. As more electron−hole pairs migrate to the surface of the semiconductor, more H_2 evolution will be obtained and a higher conversion efficiency of solar energy will be expected. Until now, less attention has been paid to the migration process of the charge carriers inside the semiconductor. In this paper, a new series of photocatalysts, $BaNi_{1/3}M_{2/3}O_3$ (M = Nb, Ta) and $BaZn_{1/3}M_{2/3}O_3$ (M = Nb, Ta), that evolve H_2 from a CH_3OH/H_2O solution with a Pt cocatalyst under UV light irradiation are reported. Raman scattering spectra of these compounds show evidence of the possible role of lattice vibrations in the photocatalytic activity of the semiconductor.

2. Experiments

Polycrystalline powders of photocatalysts $BaNi_{1/3}M_{2/3}O_3$ (M = Nb, Ta) and $BaZn_{1/3}M_{2/3}O_3$ (M = Nb, Ta) were synthesized by a solid-state reaction method. The starting materials, including $BaCO_3$, NiO, ZnO, Nb_2O_5, and Ta_2O_5 in high purity and in stoichiometric ratio, were ground and mixed thoroughly, and then preheated at 850 °C for 8 h. The preheated mixtures were reground and finally sintered at 1230 °C for 48 h.

The crystal structures of the powder samples were determined by X-ray diffraction (JEOL JDX-3500). The UV−vis diffuse reflectance spectra were measured by a UV−vis spectrophotometer (UV-2500PC Shimadzu). The surface area of the powder samples was determined by BET measurements (Gemini Micromeritics, Shimadzu). Raman spectrum measurements for the powder samples were performed using a laser Raman spectrophotometer (Jasco NRS-1000) at room temperature. The power of the incident laser beam was 100 mW with a monochromatic wavelength of 532 nm. The exposure time was 2 s. The photocatalytic reactions were performed using a closed gas circulation system. An inner-irradiation-type quartz cell with a 400-W high-pressure Hg lamp was employed. The gas that evolved was identified with a TCD gas chromatograph (Shimadzu GC-8A), which was connected to the system with a circulating line. The 0.5 wt % Pt cocatalyst was loaded onto the surface of the photocatalysts to introduce active sites.

3. Results and Discussion

3.1. Structure and UV−Vis Spectrum. Figure 1a and b shows X-ray diffraction patterns of photocatalysts $BaNi_{1/3}M_{2/3}O_3$ (M = Nb, Ta) and $BaZn_{1/3}M_{2/3}O_3$ (M = Nb, Ta). They are all well crystallized. Because of the same ionic radius of Nb^{5+} and Ta^{5+} in each pair, $BaNi_{1/3}Nb_{2/3}O_3$ and $BaNi_{1/3}Ta_{2/3}O_3$ and $BaZn_{1/3}Nb_{2/3}O_3$ and $BaZn_{1/3}Ta_{2/3}O_3$ show a similar diffraction pattern, indicating that both compounds have the same lattice parameters. In a cubic $A^{2+}B^{4+}O_3$ perovskite structure, the A^{2+} ion occupies the corner of the cubic cell, the O^{2-} ion occupies the face center, and the B^{4+} ion occupies the body center. The

* Corresponding authors. E-mail: yin.jiang@nims.go.jp and jinhua.ye@nims.go.jp.
† Japan Science and Technology Agency.
‡ ERERC, Nanjing University.
§ National Institute for Materials Science.

10.1021/jp037182e CCC: $27.50
Published on Web 06/02/2004

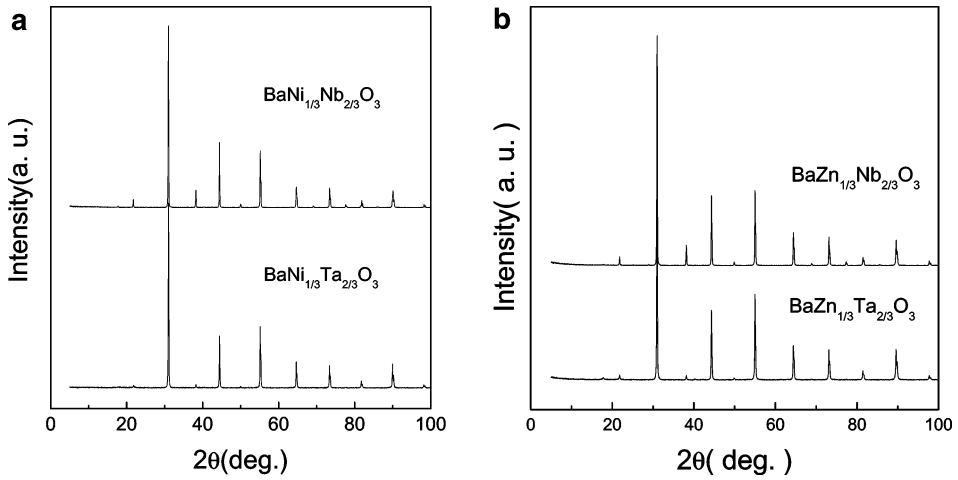

Figure 1. X-ray diffraction patterns for the pairs of the photocatalysts (a) $BaNi_{1/3}M_{2/3}O_3$ (M = Nb, Ta) and (b) $BaZn_{1/3}M_{2/3}O_3$ (M = Nb, Ta).

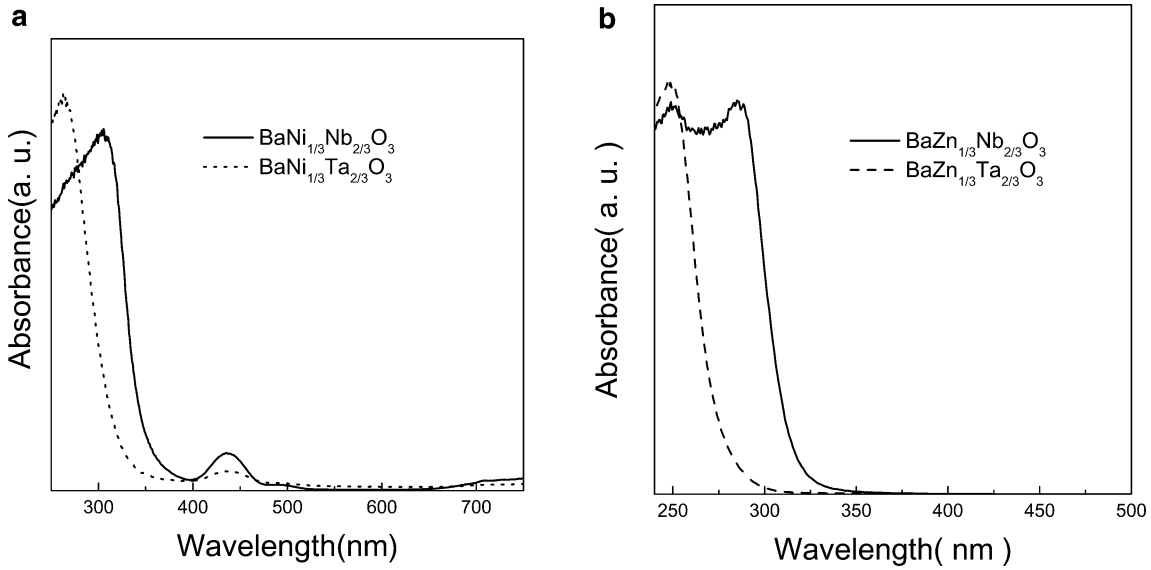

Figure 2. UV−vis diffuse reflectance spectra for the pairs of the photocatalysts (a) $BaNi_{1/3}M_{2/3}O_3$ (M = Nb, Ta) and (b) $BaZn_{1/3}M_{2/3}O_3$ (M = Nb, Ta).

neighboring octahedrons, formed by the B^{4+} and ligand O^{2-} ions, construct a 3D network by sharing their corners. In our compounds, the B site is randomly occupied by two kinds of transition-metal ions. This kind of occupation in perovskite has been widely investigated in ferroelectric materials.[6,7] Figure 2a and b shows UV−vis diffuse reflectance spectra of photocatalysts $BaNi_{1/3}M_{2/3}O_3$ (M = Nb, Ta) and $BaZn_{1/3}M_{2/3}O_3$ (M = Nb, Ta). It is obvious that for each pair, $BaNi_{1/3}Nb_{2/3}O_3$ and $BaNi_{1/3}Ta_{2/3}O_3$ and $BaZn_{1/3}Nb_{2/3}O_3$ and $BaZn_{1/3}Ta_{2/3}O_3$, in the UV light region, the Nb-containing photocatalyst shows a narrower band gap than the Ta-containing photocatalyst. By the method adopted in our previous work,[8] the band gaps of these photocatalysts corresponding to UV light absorption were determined (Table 1). The surface areas for $BaNi_{1/3}Nb_{2/3}O_3$, $BaNi_{1/3}Ta_{2/3}O_3$, $BaZn_{1/3}Nb_{2/3}O_3$, and $BaZn_{1/3}Ta_{2/3}O_3$ are 0.62, 1.27, 0.61, and 1.20 m^2/g, respectively.

3.2 Photocatalytic Activity Under UV Light Irradiation. In our experiments, the reducing reagent CH_3OH was employed to evaluate the photocatalytic activities of these photocatalysts. Figure 3a and b show the rates of H_2 evolution from the CH_3OH/H_2O solution with the 0.5 wt % Pt cocatalyst under UV light irradiation for pairs of photocatalysts $BaNi_{1/3}M_{2/3}O_3$ (M = Nb, Ta) and $BaZn_{1/3}M_{2/3}O_3$ (M = Nb, Ta), respectively. The rates of H_2 evolution from the CH_3OH/H_2O solution for these photocatalysts are listed in Table 1. After the H_2 evolution reactions were performed in the CH_3OH/H_2O solution, the crystal structures of the residues were checked again by X-ray diffraction. No additional phases could be found except the original phase, indicating that these photocatalysts were stable in the CH_3OH/H_2O solution under UV light irradiation during the experiments.

TABLE 1: Photocatalytic Activities of the Photocatalysts $BaNi_{1/3}Nb_{2/3}O_3$, $BaNi_{1/3}Ta_{2/3}O_3$, $BaZn_{1/3}Nb_{2/3}O_3$, and $BaZn_{1/3}Ta_{2/3}O_3$

compound	band gap (UV) (eV)	surface area (m^2/g)	activity (μmol H_2/h)
$BaNi_{1/3}Nb_{2/3}O_3$	3.35	0.62	68.22
$BaNi_{1/3}Ta_{2/3}O_3$	3.89	1.27	42.16
$BaZn_{1/3}Nb_{2/3}O_3$	3.82	0.61	708.21
$BaZn_{1/3}Ta_{2/3}O_3$	4.50	1.20	194.84

From Table 1, photocatalysts $BaZn_{1/3}Nb_{2/3}O_3$ and $BaZn_{1/3}Ta_{2/3}O_3$ show much higher photocatalytic activity in evolving H_2 from the CH_3OH/H_2O solution under UV light irradiation than photocatalysts $BaNi_{1/3}Nb_{2/3}O_3$ and $BaNi_{1/3}Ta_{2/3}O_3$, which may be ascribed to the unique conduction bands of $BaZn_{1/3}Nb_{2/3}O_3$ and $BaZn_{1/3}Ta_{2/3}O_3$ (Zn 4s state). For the tetrahedrally coordinated semiconductors ZnS and CdS,[9,10] special band

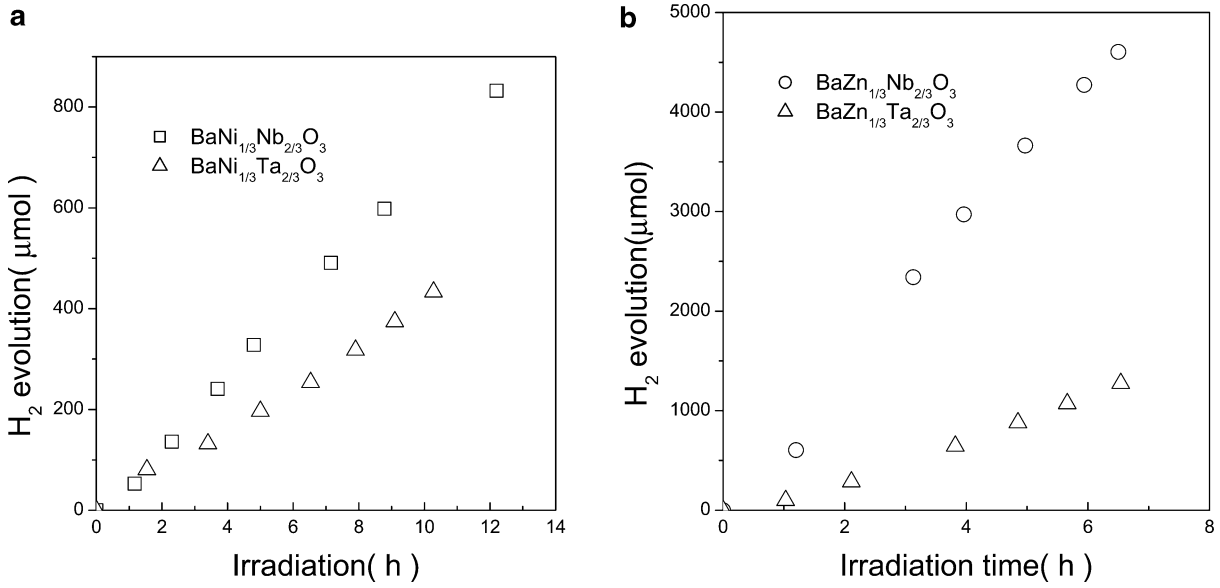

Figure 3. Rates of H_2 evolution from the CH_3OH/H_2O solution with the 0.5 wt % Pt cocatalyst under UV light irradiation for the pairs of the photocatalysts (a) $BaNi_{1/3}M_{2/3}O_3$ (M = Nb, Ta) and (b) $BaZn_{1/3}M_{2/3}O_3$ (M = Nb, Ta) (cat.: 0.5 g, co-cat.: 0.5 wt %, CH_3OH: 50 mL, H_2O: 320 mL, and Hg lamp: 400 W).

structures play an important role in their high photocatalytic activity, where the empty *n*S orbitals and the fully occupied $(n-1)$d orbitals construct their band structures. Here, in the octahedrally coordinated semiconductors $BaZn_{1/3}Nb_{2/3}O_3$ and $BaZn_{1/3}Ta_{2/3}O_3$, the conduction band (the Zn 4s state) may also dominate their high photocatalytic activity. The lower photocatalytic activity of photocatalysts $BaNi_{1/3}Nb_{2/3}O_3$ and $BaNi_{1/3}Ta_{2/3}O_3$ also could be ascribed to their special band structures. Under the crystal field of the octahedron NiO_6, the Ni 3d orbitals will split into two orbitals: t_{2g} and e_g. The following electronic occupying states should be expected: t_{2g} orbitals are fully occupied, and e_g orbitals are partially occupied. The electronic transitions from the O 2p state to the Ni e_g state and from the Ni t_{2g} state to the Nb 4d (or Ta 5d) state may correspond to the visible light absorptions in photocatalysts $BaNi_{1/3}Nb_{2/3}O_3$ and $BaNi_{1/3}Ta_{2/3}O_3$, as shown in Figure 2a, so under UV light irradiation for photocatalysts $BaNi_{1/3}Nb_{2/3}O_3$ and $BaNi_{1/3}Ta_{2/3}O_3$, some UV light photons will contribute to the orbital transition associated with the above subband gap. It is suggested that just these interband states result in the lower photocatalytic activity of the Ni compound compared to that of the corresponding Zn compound. From Figure 3a and b, it is obvious that, for the photocatalysts in each pair, the photocatalytic activity of the Nb-containing photocatalyst is always higher than that of the Ta-containing photocatalyst.

The layered perovskite photocatalyst, $Sr_2Ta_2O_7$, with a wider band gap and larger surface area, has higher photocatalytic activity under UV light irradiation than $Sr_2Nb_2O_7$.[11] A similar phenomenon also could be found in photocatalysts $InTaO_4$ and $InNbO_4$.[12] The TaO_6 and NbO_6 octahedrons in these photocatalysts suffer from different distortions, so the lattice parameters of the Nb- and Ta-containing photocatalysts are different. In the titanate family with an ABO_3 perovskite structure,[13] the titanate with a wider band gap, which is due to the different ionic radius of alkali earth metals in the A site, shows a higher photocatalytic activity under UV light irradiation, which is ascribed to the photocatalyst with a wider band gap having more powerful redox potentials. As we know, the photocatalytic activity of a semiconductor is dominated by many factors, such as the crystal structure, band gaps, lifetime of the photoproduced charge carriers, surface area, surface morphology, active site on the surface of the semiconductor, efficacy of the cocatalyst deposition, grain boundary effects, and so forth. Here in each pair, $BaNi_{1/3}Nb_{2/3}O_3$ and $BaNi_{1/3}Ta_{2/3}O_3$ and $BaZn_{1/3}Nb_{2/3}O_3$ and $BaZn_{1/3}Ta_{2/3}O_3$, both compounds have the same crystal structure and almost the same lattice parameter, although the Nb-containing photocatalyst with a narrower band gap and a smaller surface area shows a higher photocatalytic activity under UV light irradiation than the Ta-containing photocatalyst under the same reaction conditions. Therefore, it is natural for us to search for some clues from the unique scattering mechanism of charge carriers inside the Nb- and Ta-containing photocatalysts that may result in the difference in their photocatalytic activity.

The photocatalytic reaction contains three basic processes: the generation of electron−hole pairs inside the semiconductor via photoexcitation, the migration of charge carriers, and the redox reactions on the surface of the semiconductor. The migration of charge carriers to the surface of the semiconductor is quite complicated. After excitation by photons with energy higher than that of the band gap, some of the photogenerated electron−hole pairs in the semiconductor will move to the surface, and some of them will recombine. During the migration, the charge carriers will suffer scatterings from phonons and other charge carriers. It is believed that the effective separation between the photoexcited electrons and the holes will promote the migration of the charge carriers to the surface of the semiconductor, thus improving the photocatalytic activity.[14] For the above photocatalysts in each pair, although the Nb^{5+} ion has the same ionic radius as the Ta^{5+}ion, the atomic weight of Nb^{5+} is much lower than that of Ta^{5+}. The different atomic weights of the Nb^{5+} and Ta^{5+} ions will result in a different vibrational frequency in the Nb- and Ta-containing photocatalysts, so, lattice vibration may play an important role in the migration of charge carriers inside the semiconductor.

3.3. Migration Mechanism of Charge Carriers. The band structures of transition-metal oxides are generally defined by the d level of the transition metal and the 2p level of the ligand O atom.[15] For metal oxides with a d^{10} electronic configuration, the conduction band is not composed of the d level. Calculations on the band structure of ZnO using first principles show that the conduction band is composed of the Zn 4s level.[16] The tails in the long-wavelength region in Figure 2b may correspond to

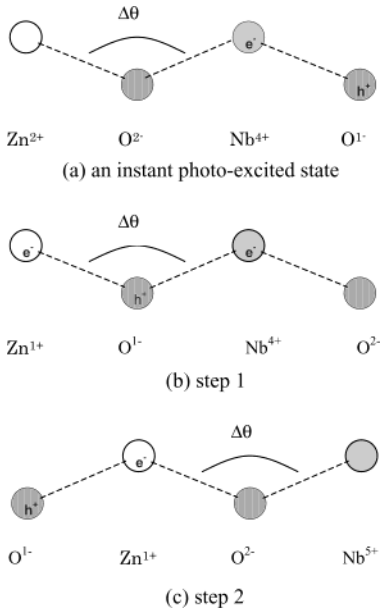

Figure 4. Schematical drawing of an instant image for the photoexcitation (a) and the subsequent charge-exchange process by two steps (b and c) in photocatalyst $BaZn_{1/3}Nb_{2/3}O_3$.

the electronic excitations from the O 2p state to the Zn 4s state. Therefore, the valence bands of $BaZn_{1/3}Nb_{2/3}O_3$ and $BaZn_{1/3}Ta_{2/3}O_3$ should be composed of the O 2p level, and the conduction bands should be composed of the Zn 4s level and the Nb 4d or Ta 5d level. As for $BaNi_{1/3}Nb_{2/3}O_3$ and $BaNi_{1/3}Ta_{2/3}O_3$ corresponding to UV light absorption, the band structures should be composed of the O 2p level and the Nb 4d level or the Ta 5d level.

For example, in $BaZn_{1/3}Nb_{2/3}O_3$ and $BaZn_{1/3}Ta_{2/3}O_3$, under the irradiation of UV light photons, the electrons in the O 2p orbitals will be excited to the Zn^{2+} 4s orbitals or the Nb^{5+} 4d (Ta^{5+} 5d) orbitals, and the holes will be left in the O 2p orbitals. In $BaZn_{1/3}Nb_{2/3}O_3$ and $BaZn_{1/3}Ta_{2/3}O_3$, bonds Zn−O, Nb−O, and Ta−O are mainly ionic, so it is impossible for the charge carriers to migrate between the Zn^{2+} and Nb^{5+} or Zn^{2+} and Ta^{5+} ions directly. Zener's[17] double-exchange mechanism of charge carriers in perovskites has been successfully applied to the conductive transport mechanism in manganese oxide.[18] Here, we assumed an instant image of the photoexcitation in $BaZn_{1/3}Nb_{2/3}O_3$, as schematically drawn in Figure 4a. The following charge-exchange processes by two steps may happen subsequently. First, one electron in the O^{2-} ion moves to the neighboring Zn^{2+} ion, as shown in Figure 4b:

$$Zn^{2+} + e^- \rightarrow Zn^+$$

and (step 1)

$$O^{2-} + h^+ \rightarrow O^-$$

Second, almost at the same time, one electron in the Nb^{4+} ion moves to the O^- ion, as shown in Figure 4c:

$$Nb^{4+} - e^- \rightarrow Nb^{5+}$$

and (step 2)

$$O^- + e^- \rightarrow O^{2-}$$

Through the above two-step processes, one electron migrates from the Nb^{4+} ion to the Zn^{2+} ion, and one hole migrates from one oxygen ion to the neighboring one. The change in the bond angle Zn−O−Nb will affect the migration of charge carriers

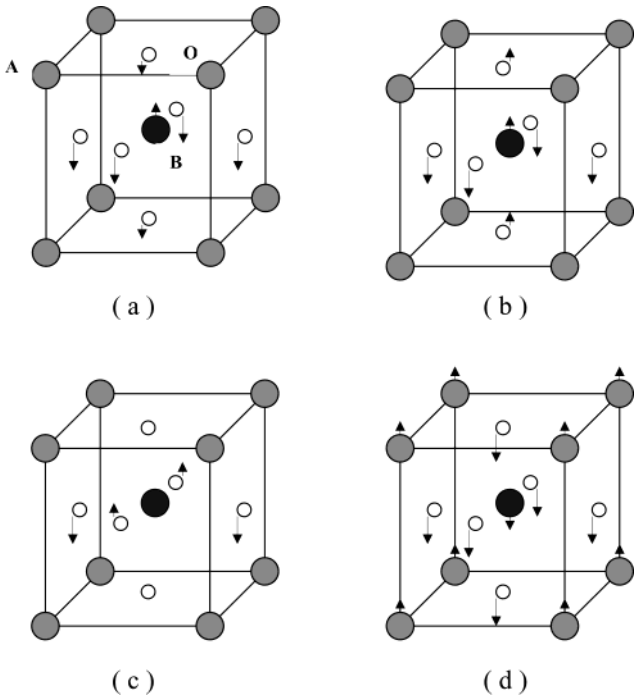

Figure 5. Optical phonon modes of the cubic perovskite ABO_3: (a) stretching; (b) bending; (c) inactive; and (d) external.

between the Zn^{2+} and Nb^{5+} ions. The migration energy of the charge carriers is proportional to the matrix element of the electronic transition t_{ij}:

$$t_{ij} = t_0 \cos\left(\frac{\Delta\vartheta_{ij}}{2}\right) \quad (1)$$

where t_0 is a constant and $\Delta\vartheta_{ij}$ is the bond angle Zn−O−Nb. Equation 1 means that the deviation of the bond angle $\Delta\vartheta_{ij}$ from 180° will increase the migration energy of the charge carriers, thus hindering the migration of the charge carriers. The above scattering mechanism of the charge carriers is also suitable for photocatalysts $BaZn_{1/3}Ta_{2/3}O_3$, $BaNi_{1/3}Nb_{2/3}O_3$, and $BaNi_{1/3}Ta_{2/3}O_3$.

3.4. Raman Scattering Spectrum. Generally, lattice dynamics is investigated by the Raman scattering spectrum and the infrared (IR) reflection spectrum. Raman scattering and IR reflection spectra of ABO_3 perovskites have been widely studied, both theoretically and experimentally.[19−21] For the cubic perovskites, the normal modes of the lattice vibration at the zone center ($k = 0$, Γ) are given in the irreducible representation by

$$\Gamma^{\text{total}} = 4F_{1u} + F_{2u} \quad (2)$$

One of the F_{1u} modes corresponding to the acoustic phonon and F_{2u} is optically silent, that is, neither IR nor Raman active, as shown in Figure 5c. The remaining three F_{1u} modes are IR active, corresponding to three vibrational motions: (i) the B−O bond distance is modulated (the stretching mode); (ii) the B−O bond angle is modulated (the bending mode); and (iii) atom A translates with respect to the BO_6 octahedron (the external mode), as schematically drawn in Figure 5a, b, and d, respectively. With the decrease of the crystal symmetry, the number of phonon modes increases in the distorted perovskite structure owing to the following two mechanisms: (1) the lowered symmetry lifts the 3-fold degenerate $F_{1u}(F_{2u})$ modes of the cubic structure and (2) the distortion enlarges the unit cell, which contains more than two formula units, and as a result, the phonon branches are folded into the reduced Brillouin zone,

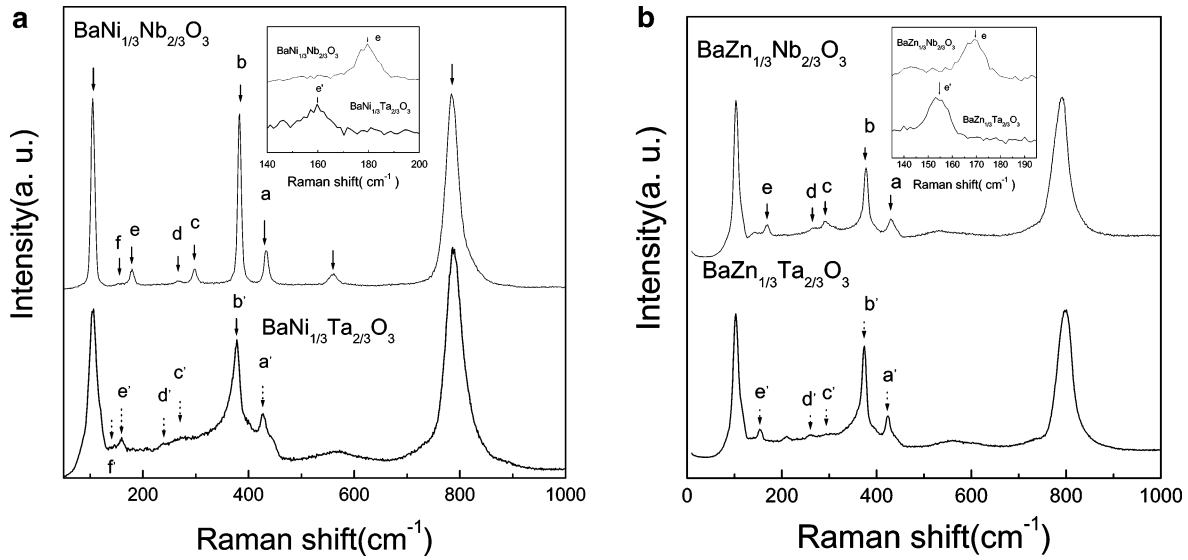

Figure 6. Raman scattering spectra of the pairs of the photocatalysts (a) $BaNi_{1/3}M_{2/3}O_3$ (M = Nb, Ta) and (b) $BaZn_{1/3}M_{2/3}O_3$ (M = Nb, Ta).

resulting in an increase in the Γ-point phonon modes. Some of the modes are Raman active, and some of them are IR active or both Raman and IR active.

Figure 6a shows Raman scattering spectra of photocatalysts $BaNi_{1/3}Nb_{2/3}O_3$ and $BaNi_{1/3}Ta_{2/3}O_3$ at room temperature. Nine phonon modes at about 105.32, 153.12, 179.53, 265.90, 297.02, 381.81, 432.64, 559.12, and 784.02 cm^{-1} could be found clearly for $BaNi_{1/3}Nb_{2/3}O_3$, and nine corresponding modes also could be found for $BaNi_{1/3}Ta_{2/3}O_3$. It was reported that $BaNi_{1/3}Nb_{2/3}O_3$ has a cubic perovskite structure.[22] As we know, no Raman active mode exists in cubic ABO_3 perovskite. The observed Raman active modes for $BaNi_{1/3}Nb_{2/3}O_3$ and $BaNi_{1/3}Ta_{2/3}O_3$ indicate that the triple-cubic perovskite structure is more reasonable for $BaNi_{1/3}Nb_{2/3}O_3$ and $BaNi_{1/3}Ta_{2/3}O_3$, as for $BaIn_{1/2}Nb_{1/2}O_3$.[23] These Raman active modes can be ascribed to the local distortion of the octahedrons due to the different ionic radii for Ni^{2+}(0.69 Å) and Nb^{5+} or Ta^{5+}(0.64 Å).

Although the complete assignment is not possible because a polarization analysis is not available, we can interpret the spectrum to be composed of three main phonon branches: the first centered around 105.32 cm^{-1}, the second branch consisting of several components around 381.81 cm^{-1}, and the third around 784.02 cm^{-1}. It is assumed that these three branches correspond to the three IR modes of the original cubic structure. The O atoms mainly move in the stretching and bending modes because the O atomic mass is much smaller than that of Ni, Nb, or Ta, so they are expected to be situated at relatively higher frequencies than for the external mode, where the Ba cation moves with respect to the NiO_6, NbO_6, or TaO_6 octahedral ensemble. Here, the three branches from lower to higher frequency are referred to as the external branch, the bending branch, and the stretching branch, respectively, according to the method adopted by Perry et al. in the IR study of perovskite.[24] Raman scattering spectra for photocatalysts $BaZn_{1/3}M_{2/3}O_3$ (M = Nb, Ta) are shown in Figure 6b. The corresponding branches also can be found for these compounds.

From Figure 6a, it is clearly found that six modes in the bending branch of $BaNi_{1/3}Ta_{2/3}O_3$ (as shown by a′, b′, c′, d′, e′, and f′) show an obvious red shift in their frequencies compared with those in $BaNi_{1/3}Nb_{2/3}O_3$ (as shown by a, b, c, d, e, and f). Compared with the e mode of $BaNi_{1/3}Nb_{2/3}O_3$, the corresponding e′ mode of $BaNi_{1/3}Ta_{2/3}O_3$ shows a red shift of about 20 cm^{-1} in its frequency, as shown by the inset in Figure 6a. From Figure 6b, similar phenomena also could be found for the pair of photocatalysts $BaZn_{1/3}M_{2/3}O_3$ (M = Nb, Ta). Compared with the e mode of $BaZn_{1/3}Nb_{2/3}O_3$, the corresponding e′ mode of $BaZn_{1/3}Ta_{2/3}O_3$ shows a red shift of about 15 cm^{-1} in its frequency, as shown by the inset in Figure 6b. The red shift in the frequencies of the bending modes in each pair of the photocatalysts may be explained by the following considerations. On one hand, the larger atomic weight of Ta^{5+} may result in lower frequencies of the bending modes in the Ta-containing photocatalysts. On the other hand, in each pair of photocatalysts, the force constants of the Ni(or Zn)−O−Ta bonds may be lower than those of the Ni(or Zn)−O−Nb bonds. As illustrated in Figure 5b, when the lattice vibrates in the bending mode, the center of the positive charge does not coincide with that of the negative charge, and the bond angle B−O−B deviates from 180°. According to eq 1, this means that the lattice vibration in the bending mode increases the migration energy of the charge carriers in the ABO_3 perovskite. For instance, in the pair $BaNi_{1/3}Nb_{2/3}O_3$ and $BaNi_{1/3}Ta_{2/3}O_3$, the softening of some modes in the bending branch of $BaNi_{1/3}Ta_{2/3}O_3$ means that the average displacement of the O^{2-} ion is larger. The bond angle Ni−O−Ta in $BaNi_{1/3}Ta_{2/3}O_3$ has more chance of deviating from 180° than the bond angle Ni−O−Nb in $BaNi_{1/3}Nb_{2/3}O_3$. In other words, the migration of charge carriers in $BaNi_{1/3}Ta_{2/3}O_3$ suffers more hindrance from lattice vibration than those in $BaNi_{1/3}Nb_{2/3}O_3$, thus leading to the higher possibility of recombination between the photogenerated electrons and holes in $BaNi_{1/3}Ta_{2/3}O_3$. Therefore, the lower photocatalytic activity is reasonable for $BaNi_{1/3}Ta_{2/3}O_3$. The same mechanism is also suitable for the pair of photocatalysts $BaZn_{1/3}M_{2/3}O_3$ (M = Nb, Ta).

4. Conclusions

In summary, two pairs of photocatalysts, $BaNi_{1/3}Nb_{2/3}O_3$ and $BaNi_{1/3}Ta_{2/3}O_3$ and $BaZn_{1/3}Nb_{2/3}O_3$ and $BaZn_{1/3}Ta_{2/3}O_3$, with the ABO_3 perovskite structure have been synthesized by the solid-state reaction process. Because of the different positions of Nb and Ta in the elemental periodic table, the Nb-containing photocatalyst in each pair shows higher photocatalytic activity than the Ta-containing photocatalyst. Raman spectra of these pairs of photocatalysts suggest that some phonon modes in the bending branches may play an important role in the migration of the photogenerated charge carriers, thus affecting the photocatalytic activity.

References and Notes

(1) Honda, K.; Fujishima, A. *Nature* **1972**, *238*, 37.
(2) Kawaii, T.; Sakata, T. *Nature* **1980**, *286*, 474.
(3) Zou, Z.; Ye, J.; Sayama, K.; Arakawa, H. *Nature (London)* **2001**, *414*, 625.
(4) Shapovalov, V.; Stefanovich, E. V.; Truong, T. N. *Surf. Sci.* **2002**, *498*, L103.
(5) Henderson, M. A.; Epling, W. S.; Peden, C. H. F.; Perkins, C. L. *J. Phys. Chem. B* **2003**, *107*, 534.
(6) Gao, X. S.; Chen, X. Y.; Yin, J.; Wu, J.; Liu, Z. G. *J. Mater. Sci.* **2000**, *35*, 5421.
(7) Goodenough, J. B.; Lango, J. M. Landolt-Boorstein Tabellen, New series. Vol. III/4a, Springer: Berlin, 1970.
(8) Yin, J.; Zou, Z.; Ye, J. *J. Phys. Chem. B* **2003**, *107*, 4936.
(9) Reber, J. F.; Meier, K. *J. Phys. Chem.* **1984**, *88*, 5903.
(10) Sato, T.; Masaki, K.; Yoshioka, T.; Okuwaki, A. *J. Chem. Technol. Biotechnol*. **1993**, *58*, 315.
(11) Yoshino, M.; Kakihana, M.; Cho, W. S.; Kato, H.; Kudo, A. *Chem. Mater.* **2002**, *14*, 3369.
(12) Zou, Z.; Ye, J.; Arakawa, H. *Chem. Phys. Lett.* **2000**, *332*, 271.
(13) Oosawa, Y.; Takahashi, R.; Yonemura, M.; Sekine, T.; Goto, Y. *New J. Chem.* **1989**, *13*, 435.
(14) Linsebigler, A. L.; Lu, G.; Yates, J. T., Jr. *Chem. Rev.* **1995**, *95*, 735.
(15) Scaife, D. E. *Sol. Energy* **1980**, *25*, 41.
(16) Sato, K.; Yoshida, H. K. *Jpn. J. Appl. Phys.* **2001**, *40*, L334.
(17) Zener, C. *Phys. Rev.* **1951**, *82*, 403.
(18) Urushibara, A.; Moritomo, Y.; Arima, T.; Asamitsu, A.; Kdo, G.; Tokura, Y. *Phys. Rev. B* **1995**, *51*, 14103.
(19) Fontana, M. D.; Metrat, G.; Servoin, J. L.; Gervais, F. *J. Phys. C: Solid State Phys.* **1984**, *16*, 483.
(20) Scalabrin, A.; Chaves, A. S.; Shim, D. S.; Porto, S. P. S. *Phys. Status Solidi B* **1977**, *79*, 731.
(21) Souza Filho, A. G.; Lima, K. C. V.; Ayala, A. P.; Guedes, I.; Freire, P. T. C.; Melo, F. E. A.; Mendes Filho, J.; Araujo, E. B.; Eiras, J. A. *Phys. Rev. B* **2002**, *66*, 132107.
(22) Roy, R. *J. Am. Ceram. Soc.* **1954**, *37*, 581.
(23) Galasso, F.; Darby, W. *J. Phys. Chem.* **1962**, *66*, 131.
(24) Perry, C. H.; Khanna, B. N. *Phys. Rev. A* **1964**, *135*, 408.